ISSN 1063-7737, Astronomy Letters, 2014, Vol. 40, No. 12, pp. 800–820. © Pleiades Publishing, Inc., 2014.
Original Russian Text © I.A. Usenko, A.Yu. Kniazev, L.N. Berdnikov, V.V. Kravtsov, 2014, published in Pis'ma v Astronomicheskiĭ Zhurnal, 2014, Vol. 40, No. 12, pp. 857–877.

Spectroscopic Studies of Cepheids in Circinus (AV Cir, BP Cir) and Triangulum Australe (R TrA, S TrA, U TrA, LR TrA)

I. A. Usenko[1*], A. Yu. Kniazev[2,3,4], L. N. Berdnikov[4], and V. V. Kravtsov[5,4]

[1] *Astronomical Observatory, Odessa National University, Shevchenko park, Odessa, 65014 Ukraine*
[2] *South African Astronomical Observatory, P. O. Box 9, Observatory, Cape Town, 7935 South Africa*
[3] *Southern African Large Telescope, P. O. Box 9, Observatory, Cape Town, 7935 South Africa*
[4] *Sternberg Astronomical Institute, Lomonosov Moscow State University, Universitetskii pr. 13, Moscow, 119991 Russia*
[5] *Departamento de Fisica, Facultad de Ciencias Naturales, Universidad de Atacama, Copayapu 485, Copiapo, Chile*

Received June 11, 2014

Abstract—Based on high-resolution spectra taken with the 1.9-m telescope of the South African Astronomical Observatory, we have determined the atmospheric parameters and chemical composition for three small-amplitude (AV Cir, BP Cir, and LR TrA), two classical (R TrA and S TrA), and one double-mode (U TrA) Cepheids. The averaged atmospheric parameters have been estimated for three Cepheids (AV Cir, BP Cir, and U TrA) observed at various pulsation phases. In all Cepheids, except U TrA, the metallicity has turned out to be higher than the solar one by 0.1–0.2 dex. The abundances of the key elements of the evolution of yellow supergiants (C, O, Na, Mg, Al) show that these objects have already passed the first dredge-up, while those of the remaining elements are nearly solar. Comparison of our results on the Cepheids from the list (except U TrA) with those of other authors shows significant differences in C and O abundance estimates for AV Cir, R TrA, S TrA, and LR TrA. For AV Cir and BP Cir, the Hα line profiles are symmetric but with a slight asymmetry in the core at approximately the same phase near $0\overset{P}{.}7$: on the "blue" side for AV Cir and on the "red" one for BP Cir. BP Cir exhibits a distinct asymmetry in the absorption lines of neutral atoms and ions at various pulsation phases, which can be explained by nonradial *first-overtone* pulsations. The constancy of the Hα absorption line profiles with pulsation phase for AV Cir and BP Cir may suggest the presence of a hydrogen envelope around them. For the double-mode Cepheid U TrA, an asymmetry is observed in the cores of the Hα line and the absorption lines of neutral atoms and ions at various pulsation phases, which can be explained by nonradial pulsations in the Cepheid's atmosphere. The absorption lines of neutral atoms and ions of metals in LR TrA closely resemble those in the well-known Cepheid BG Cru: secondary "blue" and "red" components whose line depths vary with pulsation phase are noticeable. This Cepheid can also pulsate in the *first overtone* and have an extended hydrogen envelope. Careful multiphase spectroscopic observations with a sufficiently high resolution are needed to test this assumption.

DOI: 10.1134/S1063773714110061

Keywords: *Cepheids, spectra, atmospheric parameters, chemical composition, circumstellar envelopes.*

INTRODUCTION

We present the next paper devoted to the studies of southern-hemisphere variable yellow supergiants based on our observations performed at the South African Astronomical Observatory. We formulated the main goals and tasks of these studies, determining the atmospheric parameters and chemical composition of these objects, in the first part (Berdnikov et al. 2010). The first results for six classical Cepheids are also presented there. In our succeeding papers (Usenko et al. 2011, 2013, 2014), we obtained similar estimates for seventeen more classical Cepheids and three bright supergiants falling into the Cepheid instability strip. We revealed at least two small-amplitude Cepheids with a hydrogen envelope, one of which is a first-overtone pulsator. The detection of such objects extended the range of problems for our studies. We are now trying to reveal the possible

*E-mail: igus99@ukr.net

presence of such envelopes around all of the classical Cepheids in the Galaxy under study using spectral methods. Recently, based on non-LTE calculations of the C, N, O, and Na abundances in the atmospheres of 12 Cepheids, Takeda et al. (2013) confirmed the validity of our method for determining the microturbulent velocity V_t from the condition for the abundance for Fe II lines being independent of their equivalent widths. As a result, no significant spread in the abundances of the key elements of the evolution of yellow supergiants, especially for oxygen, is observed in our works.

We have already investigated the classical Cepheid S TrA in our second paper (the results of our abundance analysis based on one spectrum), while the spectroscopic studies for the other variable R TrA are being carried out for the first time. The objects LR TrA, AV Cir, and BP Cir belong to the class of small-amplitude or s-Cepheids (DCEPS), while U TrA is a double-mode Cepheid (CEP(B)).

OBSERVATIONS AND PRIMARY REDUCTION

Our observations were performed in August, 2011 with the GIRAFFE (Grating Instrument for Radiation Analysis with a Fiber Fed Echelle) fiber echelle spectrograph mounted at the Coude focus of the 1.9-m telescope at the South African Astronomical Observatory (SAAO, South African Republic). We took 13 spectra for all six Cepheids: three for AV Cir and BP Cir, one for R TrA, S TrA, and LR TrA, and four for U TrA.

To improve the quality of our spectroscopic data, two or three spectra in succession were taken for each object, except R TrA and S TrA, on each observing night (with the same exposure time), which were summed after the primary reduction.

Information about the objects and some details of our observations are presented in Table 1. Its columns from the first to the eighth give, respectively, the object name, its equatorial coordinates α and δ (epoch 2000), the period P of brightness variations from GCVS-4 (Kholopov et al. 1986), the mean V magnitude taken from the catalog by Berdnikov et al. (2000), the exposure time, the heliocentric radial velocities V_r that we determined from the spectra described in this paper together with their errors, the mid-exposure heliocentric Julian date HJD, and the summed signal-to-noise ratio. The signal-to-noise ratio for wavelengths in the range 5000–6000 Å was calculated using a robust AMD (Absolute Mean Deviation) estimate (Kniazev et al. 2004) for each of the individual spectra. The corresponding signal-to-noise ratio for each summed spectrum was calculated as $\sqrt{n}$(S/N), where n is the number of individual spectra and S/N is the signal-to-noise ratio for an individual spectrum (this value was assumed to be approximately the same).

As has already been mentioned in our previous papers (Berdnikov et al. 2010; Usenko et al. 2011, 2013), GIRAFFE is a copy of the MUSICOS spectrograph designed at the Meudon observatory (Baudrand and Böhm 1992) and allows high-resolution ($R = 39\,000$) echelle spectra to be obtained in the spectral range 3820–10 400 Å. For our observations, we used a prism optimized for the spectral range 5200–10 400 Å and an optical fiber with a diameter of 50 μm. The detector was a 1024×1024-pixel TEK6 CCD camera. The total recorded spectral range (4250–7100 Å) contained 52 spectral orders. The spectral range used for our analysis was 4300–7100 Å for R TrA and S TrA and 4250–6750 Å for the remaining four objects.

The full process of taking spectra and reducing CCD images is described in detail in our previous papers (Berdnikov et al. 2010; Usenko et al. 2011, 2013). As has been said above, to increase the signal-to-noise ratio and to remove cosmic-ray particle hits, we summed two (or three) spectra of the same object taken in succession followed by median filtering.

We determined the radial velocities using the cross-correlation technique in the XSPEC2 software package designed for GIRAFFE echelle spectra (Balona 1999). The accuracy of determining V_r is 0.1–0.3 km s^{-1}.

We reduced the spectra with the DECH 20 software package (Galazutdinov 1992). The equivalent widths of absorption lines for all objects, except LR TrA, were measured either by Gaussian fitting or by direct integration. Only for LR TrA did we use only direct integration because of its complex absorption line profiles.

MODEL PARAMETERS

To calculate the chemical composition of a star, it is first necessary to determine its effective temperature $T_{\rm eff}$, surface gravity $\log g$, and microturbulent velocity V_t. The effective temperatures $T_{\rm eff}$ were determined by a method based on the depth ratios of selected pairs of spectral lines most sensitive to the temperature. Several spectroscopic criteria (Kovtyukh 2007) were used in this case. This method provides an internal accuracy of $\sim$20 K for $T_{\rm eff}$ (the error of the mean). The microturbulent velocity V_t was determined from the condition for the Fe II abundance derived from a set of lines being independent of their equivalent widths (Kovtyukh and Andrievsky 1999). The surface gravity $\log g$ was determined from

Table 1. Information about the objects and observations

Cepheid	α (2000.0)	δ (2000.0)	V, mag	P, days	Exposure time, min	V_r, km s^{-1}	HJD 2450000+	S/N ratio
AV Cir	14 50 30.3	−67 29 51	7.44	3.06	60	-0.49 ± 0.10	5788.3305	68
					60	$+8.51 \pm 0.10$	5789.3419	49
					60	$+8.36 \pm 0.09$	5790.3372	55
BP Cir	14 46 42.0	−61 27 43	7.56	2.40	60	-9.13 ± 0.11	5788.3680	35
					60	-24.09 ± 0.17	5789.2813	57
					60	$+8.36 \pm 0.09$	5790.3372	55
R TrA	15 19 45.7	−66 29 46	6.66	3.39	20	$+1.74 \pm 0.16$	5675.5354	89
S TrA	16 01 10.7	−63 46 35	6.40	6.32	40	$+28.68 \pm 0.14$	5790.2580	85
U TrA	16 07 19.0	−62 54 38	7.89	2.57	60	$+0.31 \pm 0.11$	5784.3244	23
					60	-13.05 ± 0.10	5785.2752	30
					40	$+3.80 \pm 0.09$	5787.3440	30
					60	-37.42 ± 0.16	5788.2297	62
LR TrA	15 30 49.8	−65 35 58	7.81	2.46	60	-28.45 ± 0.20	5789.4047	35

the ionization equilibrium condition for Fe I and Fe II atoms.

The atmospheric parameters we determined for the summed spectra are listed in Table 2. It also provides the calculated times of maxima and pulsation periods. When estimating the atmospheric parameters and chemical composition, we used the solar oscillator strengths (Kovtyukh and Andrievsky 1999) and model atmospheres from Kurucz (1992). More detailed information about the methods of determining the atmospheric parameters of our program stars and their measurement errors is given in our previous paper (Berdnikov et al. 2010).

CHEMICAL COMPOSITION

We determined the chemical composition of the program stars in the LTE approximation using the WIDTH9 code and a grid of models from Kurucz (1992). Tables 3–10 present the derived elemental abundances relative to the Sun [El/H] with their errors σ and give the number of lines NL used for each element. Complete information about the influence of uncertainties in determining the atmospheric parameters on the elemental abundance estimates was provided in our previous paper (Berdnikov et al. 2010).

DISCUSSION

For all Cepheids from our list, except U TrA, the chemical composition was analyzed by Luck and Lambert (2011) (below referred to as LL) and Luck et al. (2011) (below referred to as LAKGG) based on the spectroscopic data (one spectrum for each object) obtained in 2010 with the 2.2-m MPG/ESO telescope (La Silla, Chile) with a resolution of 48 000 and a S/N ratio of more than 100. In both papers, the

Table 2. Atmospheric parameters and light elements for the program Cepheids

Object	Spectrum number	HJD 2450000+	$T_{\rm eff}$, K	$\log g$	V_t, km s^{-1}	Time of max. 2450000+	Period, days	Phase
AV Cir	1080186	5788.3305	6308 ± 17	2.30	4.20	5113.6504	3.065221	0.108
	1080231	5789.3419	5928 ± 17	2.10	3.80			0.438
	1080278	5790.3372	6244 ± 20	2.50	4.00			0.763
BP Cir	1080192	5788.3680	6296 ± 29	2.70	4.20	5112.7112	2.398131	0.743
	1080225	5789.2813	6579 ± 19	2.80	3.60			0.124
	1080272	5790.3372	6193 ± 22	2.75	3.90			0.564
R TrA	1010067	5675.5354	5852 ± 21	2.10	4.50	3117.4856	3.389194	0.766
S TrA	1010069	5675.5575	5582 ± 20	1.90	5.20	3115.8471	6.323585	0.788
U TrA	1080030	5784.3244	–	–	–	5122.8479	2.568443	0.540
	1080101	5785.2752	6101 ± 24	2.00	3.80			0.910
	1080156	5787.3440	5577 ± 36	1.70	3.70			0.716
	1080177	5788.2297	6576 ± 27	2.30	4.10			0.060
LR TrA	1080237	5789.4047	5792 ± 17	1.70	4.50	5123.3816	2.428286	0.277

authors used different techniques for estimating the atmospheric parameters and chemical composition, which affected the results (they are presented below in the text and tables for comparison).

AV Cir. This is a small-amplitude Cepheid (DCEPS) of spectral type F7 II. It was investigated mainly photometrically (Eggen 1985a, 1985b; Berdnikov and Turner 2001). Only McAllary and Welch (1986) detected a slight infrared excess in the Cepheid during its IRAS observations and established its mean $T_{\rm eff} = 6220$ K.

For one spectrum taken at phase $0^P.207$, LL provide the atmospheric parameters $T_{\rm eff} = 6156 \pm 50$ K, $\log g = 2.53$, and $V_t = 3.61$ km s^{-1}, while LAKGG give $T_{\rm eff} = 6169 \pm 56$ K, $\log g = 2.10$, and $V_t = 3.30$ km s^{-1}. We took three spectra at different phases of the light curve and, judging by the phase, the LAKGG results for $T_{\rm eff}$ and $\log g$ roughly correspond to intermediate values between our spectra 1 080 186 and 1 080 231 (see Table 2). The mean atmospheric parameters from our data are $T_{\rm eff} = 6160 \pm 18$ K, $\log g = 2.30$, and $V_t = 4.00$ km s^{-1}, respectively.

Figure 1 presents the Hα line profiles for the Cepheid AV Cir at various pulsation phases. As can be seen from the figure, the line profiles are symmetric at phases $0^P.108$ and $0^P.438$ and only at phase $0^P.763$ is the line core slightly asymmetric on the "blue" side. Previously (Usenko et al. 2014), using the small-amplitude Cepheid BG Cru as an example, we showed the changes of the Fe I 6055.99 Å line profile and the Fe II 6369.46 Å and Si II 6371.355 Å absorption line profiles with pulsation phase. A noticeable asymmetry of the profiles and the appearance of additional blue and red components were observed

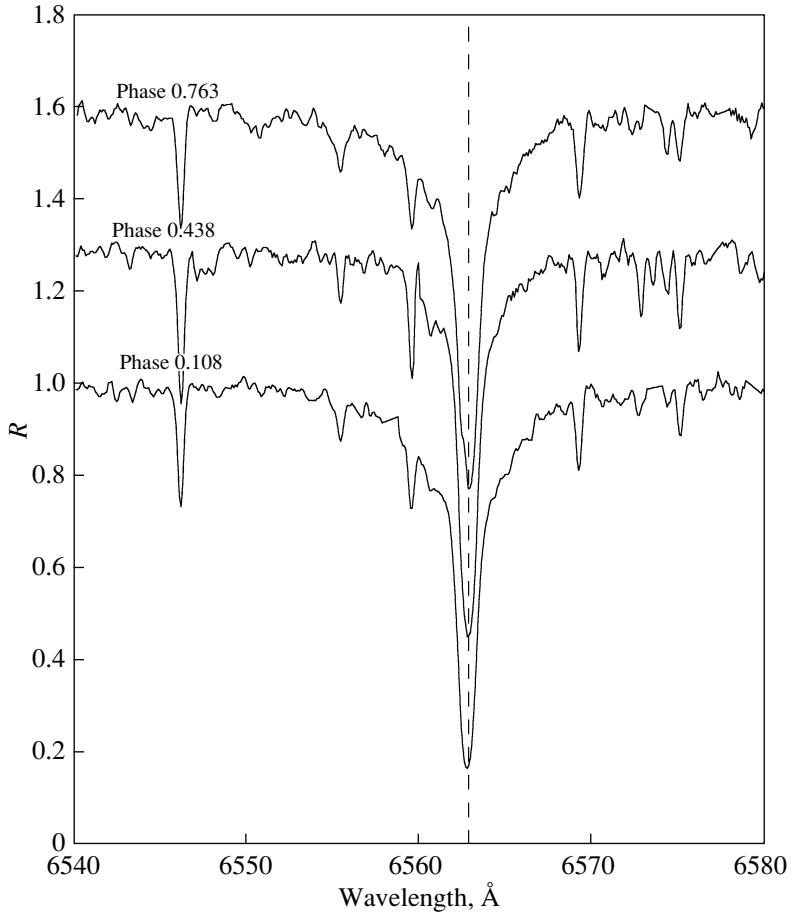

Fig. 1. Change of the Hα line profile with pulsation phase for AV Cir.

in these lines, which was explained by the presence of nonradial pulsations and (or) the presence of an extended circumstellar envelope. AV Cir exhibits no noticeable asymmetry and no additional components in the absorption lines of neutral atoms and ions.

Table 3 lists the abundances of chemical elements in the atmosphere of AV Cir for each spectrum. Table 4 gives the values averaged over our three spectra and, separately, the results from LL and LAKGG for comparison. As can be seen from Table 4, our results obtained from spectrograms with a half as much signal-to-noise ratio and a lower resolution show good agreement with the results on iron: [Fe/H] = +0.13 dex. As regards the key elements of the evolution of yellow supergiants, here we see a clear mismatch in carbon abundance estimates: a noticeable underabundance [C/H] = −0.22 dex according to our data and a nearly solar abundance in LL and LAKGG. There are significant discrepancies between the results of both groups of authors for oxygen and the LAKGG result may be considered close to our data. As regards the sodium, magnesium, and aluminum abundance estimates, they are rather close, except for the slight Al overabundance in our results.

The abundances of the α-elements are approximately identical (except for the sulfur overabundance in LAKGG); the same can also be said about the iron-peak elements. For the r-process elements and heavy and light s-process elements, there are differences only in zinc and europium abundances. On the whole, however, the abundances of all these elements are nearly solar. If we take our results on the carbon and oxygen abundances as the main ones and add the LL and LAKGG estimates for nitrogen ([N/H] $\approx$ +0.5 dex) to them, then it can be concluded that the Cepheid AV Cir has already passed the first dredge-up.

BP Cir. This is a small-amplitude Cepheid (DCEPS) of the unexpectedly early spectral type F2/3 II (Olsen 1979). Kurtz (1979) pointed out that the star is similar in its spectral lines to a δ Sct variable. Analyzing the radial velocity curve, Balona (1981) concluded that this variable is a small-amplitude Cepheid pulsating in the *first overtone*. This assumption was confirmed by Arel-

Table 3. Elemental abundances for AV Cir

Species	1 080 186			1 080 231			1 080 278		
	[El/H]	σ	NL	[El/H]	σ	NL	[El/H]	σ	NL
C I	−0.24	0.20	11	−0.20	0.23	12	−0.23	0.10	9
O I	+0.09	0.26	4	−0.02	0.23	4	+0.01	0.05	3
Na I	+0.22	0.20	7	+0.23	0.17	6	+0.12	0.20	6
Mg I	-0.04	0.32	5	−0.09	0.35	5	−0.05	0.13	5
Al I	+0.34	0.13	2	+0.40	0.03	2	+0.27	0.01	2
Si I	+0.13	0.10	20	+0.15	0.13	21	+0.15	0.09	19
Si II	–	–	–	–	–	–	+0.06	0.29	2
S I	+0.02	0.14	5	+0.27	0.29	4	−0.13	0.14	5
Ca I	+0.03	0.20	16	−0.07	0.19	13	+0.11	0.17	16
Sc I	−0.26	–	1	−0.01	0.18	3	+0.17	0.01	2
Sc II	+0.02	0.17	8	−0.06	0.17	9	−0.06	0.22	9
Ti I	+0.07	0.17	58	+0.04	0.19	52	+0.06	0.19	43
Ti II	−0.00	0.16	15	−0.04	0.13	12	+0.04	0.12	15
V I	+0.11	0.20	14	+0.12	0.15	21	+0.07	0.15	12
V II	+0.12	0.21	6	+0.06	0.23	6	+0.12	0.07	2
Cr I	+0.09	0.24	58	+0.11	0.23	58	+0.02	0.22	47
Cr II	+0.09	0.16	15	+0.04	0.13	15	+0.10	0.16	14
Mn I	−0.10	0.14	12	−0.06	0.20	17	−0.08	0.16	17
Fe I	+0.13	0.15	206	+0.15	0.18	215	+0.13	0.15	170
Fe II	+0.13	0.14	46	+0.15	0.12	37	+0.12	0.08	36
Co I	+0.05	0.19	26	-0.03	0.17	24	+0.01	0.19	18
Ni I	+0.02	0.19	93	−0.03	0.17	88	+0.01	0.19	90
Cu I	+0.30	0.31	4	+0.29	0.13	4	+0.18	0.27	4
Zn I	−0.21	0.38	4	−0.17	0.48	3	−0.31	0.19	4
Sr I	–	–	–	−0.06	0.63	2	+0.28	–	1
Y I	–	–	–	+0.26	–	1	–	–	–
Y II	+0.23	0.16	8	+0.11	0.22	7	+0.21	0.14	7
Zr II	+0.15	0.28	6	+0.13	0.19	5	+0.27	0.24	6
La II	+0.18	0.22	7	+0.05	0.38	6	+0.17	0.20	6
Ce II	+0.10	0.23	14	+0.08	0.20	14	+0.04	0.14	10
Pr II	-0.20	0.03	3	−0.19	0.10	3	−0.02	0.10	2
Nd II	+0.09	0.22	18	+0.05	0.23	16	+0.19	0.20	15
Sm II	+0.02	0.09	4	+0.53	0.11	2	−0.25	0.10	3
Eu II	+0.31	0.22	2	+0.05	–	1	+0.20	0.08	2
Gd II	–	–	–	+0.47	–	1	+0.44	–	1

Table 4. Averaged elemental abundances for AV Cir

Species	Our paper			LL	LAKGG
	[El/H]	σ	NL	[El/H]	[El/H]
C I	−0.22	0.18	32	−0.01	−0.06
O I	+0.03	0.19	11	+0.33	−0.08
Na I	+0.17	0.17	21	+0.21	+0.24
Mg I	−0.06	0.27	15	+0.09	+0.03
Al I	+0.34	0.07	6	+0.13	+0.16
Si I	+0.14	0.11	60	+0.15	+0.17
Si II	+0.06	0.29	2	–	–
S I	+0.10	0.18	24	–	+0.26
Ca I	+0.03	0.16	45	−0.01	+0.04
Sc I	+0.01	0.09	6	–	+0.04
Sc II	−0.03	0.19	26	–	–
Ti I	+0.06	0.18	153	+0.17	+0.14
Ti II	+0.00	0.14	42	–	–
V I	+0.10	0.16	47	–	+0.01
V II	+0.09	0.20	14	–	–
Cr I	+0.08	0.23	163	+0.02	+0.05
Cr II	+0.08	0.15	44	–	–
Mn I	−0.08	0.17	46	−0.13	−0.01
Fe I	+0.13	0.16	591	+0.13	+0.10
Fe II	+0.13	0.13	119	–	–
Co I	+0.04	0.19	68	+0.09	+0.06
Ni I	+0.00	0.18	271	−0.04	+0.06
Cu I	+0.26	0.24	12	–	+0.09
Zn I	−0.23	0.34	11	–	−0.01
Sr I	+0.05	0.42	3	–	–
Y I	+0.26	–	1	+0.32	+0.20
Y II	+0.18	0.17	22	–	–
Zr II	+0.19	0.23	17	–	+0.14
La II	+0.14	0.26	19	+0.32	+0.00
Ce II	+0.08	0.19	38	+0.21	+0.12
Pr II	−0.15	0.07	8	+0.11	−0.04
Nd II	+0.11	0.22	49	+0.24	−0.02
Sm II	+0.04	0.10	9	+0.19	−0.05
Eu II	+0.21	0.12	5	+0.13	+0.07
Gd II	+0.46	–	2	–	–

LL—data from Luck and Lambert (2011); LAKGG—data from Luck et al. (2011).

lano Ferro (1984). Thereafter, Arellano Ferro and Madore (1985) detected a companion of spectra type B4–B5 V with the atmospheric parameters $T_{\rm eff} = 16\,000 \pm 1000$ K and $\log g = 4.0 \pm 0.5$ in the Cepheid after its IUE observations. The absolute magnitude of the Cepheid M_V was estimated to be $-2\overset{m}{.}8$ for the case of a *fundamental-mode* pulsation and $-3\overset{m}{.}0$ in the *first overtone*. Subsequently, Evans et al. (1992) and Evans (1994) showed the companion's spectral type to be B6 V and the Cepheid's effective temperature to be ∼6310 K. The evolutionary model of the Cepheid calculated from the opacities of Iglesias and Rogers (1991) for a *first-overtone* pulsation showed that it had no convective mixing in the core. The absolute magnitudes in the case of *fundamental-mode* and *first-overtone* pulsations are $-2\overset{m}{.}39$ and $-2\overset{m}{.}93$, respectively. The studies by Petterson et al. (2004) showed that the orbital period of the companion is rather difficult to estimate, but it is probably very long. The Cepheid's mass was estimated to be 4.4 and 5.0 $M_\odot$ for the *fundamental mode* and the *first overtone*, respectively. The subsequent studies of the radial velocities based on various hydrogen lines and lines of neutral metals and ions performed by Petterson et al. (2005) revealed an interaction between two pressure waves corresponding to *fundamental-mode* and *first-overtone* pulsations and passing through the Cepheid's atmosphere. The same authors assumed BP Cir to pulsate in the *overtone*.

The atmospheric parameters of the Cepheid derived from only one spectrum at phase $0\overset{P}{.}033$ in LL and LAKGG are: $T_{\rm eff} = 6543 \pm 67$ and 6533 ± 76 K, $\log g = 2.62$ and 2.40, and $V_t = 3.36$ and 3.70 km s^{-1}, respectively. It can be seen that the spectrum was taken near maximum light and the effective temperatures are close to the value obtained for our spectrum 1 080 225 at phase $0\overset{P}{.}124$ (see Table 2). There is good agreement with the microturbulent velocity, but the surface gravity for our spectrum is noticeably larger. If we add our effective temperatures, then we will obtain the mean $T_{\rm eff} = 6356 \pm 23$ K, which is close to the estimate from Evans (1994). The mean estimates of $\log g$ and V_t are 2.75 and 3.90 km s^{-1}, respectively. It should be noted that the mean surface gravity estimate is rather high for the *first overtone*: for example, for the Cepheid SU Cas with a close $T_{\rm eff} = 6345 \pm 30$ K, the mean estimate is $\log g = 2.40$ (Usenko et al. 2013a).

Figure 2 presents the Hα line profiles for various pulsation phases. Just as for AV Cir, the line profiles are also symmetric at phases $0\overset{P}{.}124$ and $0\overset{P}{.}564$. However, a slight asymmetry of the line core, but on the "red" side, is also observed at phase $0\overset{P}{.}743$. As regards the absorption lines of neutral atoms and ions,

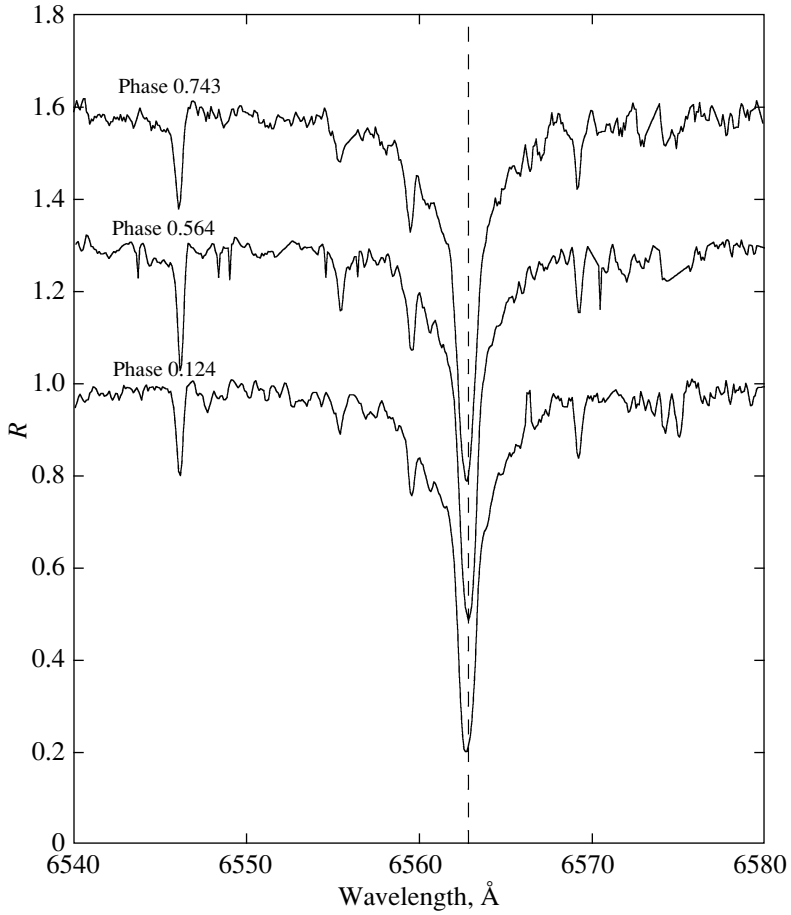

Fig. 2. Change of the Hα line profile with pulsation phase for BP Cir.

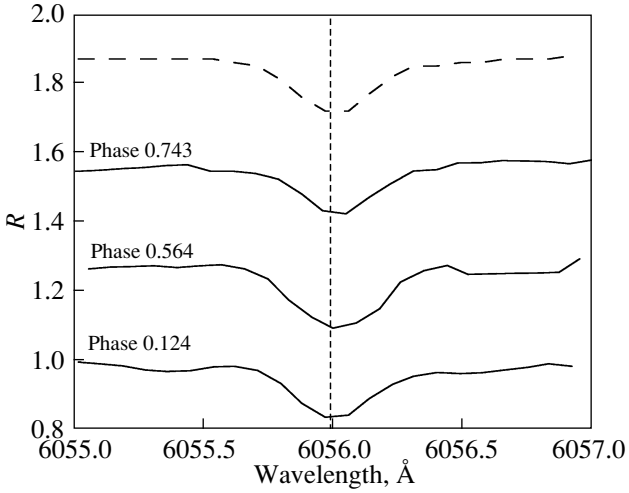

Fig. 3. Change of the Fe I 6055.99 Å absorption line profile with pulsation phase for BP Cir. The averaged line profile obtained from our observational data is indicated by the dashed line in the upper part of the figure.

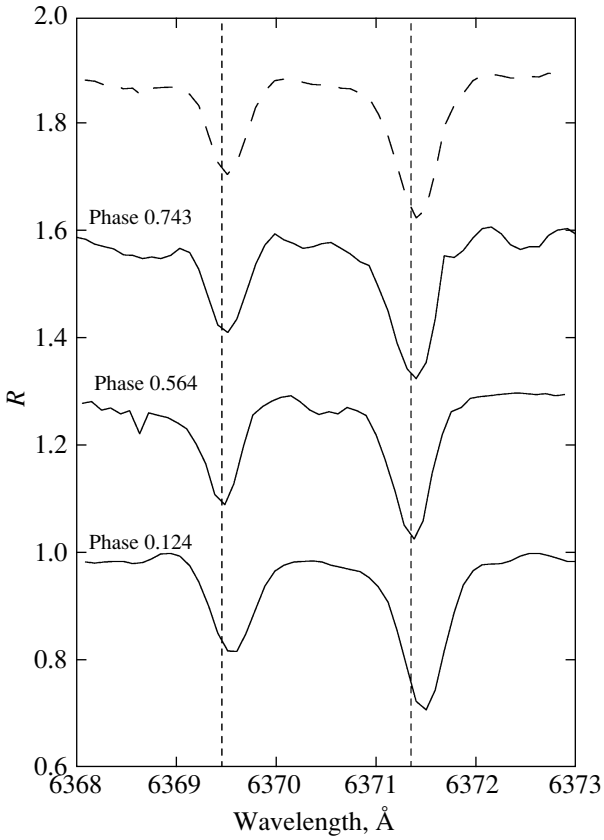

Fig. 4. Change of the Fe II 6369.46 Å and Si II 6371.355 Å absorption line profiles with pulsation phase for BP Cir. The averaged line profile obtained from our observational data is indicated by the dashed line in the upper part of the figure.

their asymmetric shape and its change with pulsation phase are clearly seen (see the Fe I 6055.99 Å and Fe II 6369.46 Å and Si II 6371.355 Å lines in Figs. 3 and 4). This is especially clearly seen for the Fe I line at phase $0\overset{P}{.}564$; the presence of a "red" component is not ruled out, as in the case of BG Cru. The ion line cores at phase $0\overset{P}{.}124$ exhibit a redshift. It is quite probable that this can be explained by a manifestation of the interaction between two pressure waves for two overtones as was explained by Petterson et al. (2005) or nonradial *first-overtone* pulsations.

The results of our abundance determinations for BP Cir are presented in Tables 5 and 6. When the chemical composition of the Cepheid is analyzed, attention should be paid to the iron abundance [Fe/H] = +0.13 dex, which is similar to that for AV Cir (Table 4) but differs greatly from the LL and LAKGG data (Table 6). The carbon abundance is also close to AV Cir and this estimate agrees well with LL and LAKGG, but our estimate for the oxygen abundance close to AV Cir differs noticeably from LL and LAKGG. The estimates roughly coincide for sodium and magnesium, are close to AV Cir for aluminum, but are larger than those in LL and LAKGG.

The abundances for the α-elements and Fe-peak elements are approximately identical. Only the cobalt abundance constitutes an exception: LAKGG revealed an underabundance. For the r-process elements and heavy and light s-process elements, there are differences only in praseodymium and samarium abundances. Just as for AV Cir, the abundances of all these elements are also nearly solar. If we take, just as for AV Cir, our results on the carbon and oxygen abundances as the main ones and add the LL and LAKGG estimates for nitrogen ([N/H] $\approx$ +0.34 dex) to them, then it can also be concluded that the Cepheid BP Cir has passed the first dredge-up.

R TrA. This is a classical Cepheid of spectral type F7 Ib–II with a short period. Schmidt (1970) investigated one spectrum with the Hα line profile taken near maximum light. The line profile turned out to be symmetric, without any emission and splitting in the core. The Cepheid was investigated by the maximum likelihood method (Balona 1977; Balona and Stobie 1979b): it is a radial pulsator with a mean radius $35.8 \pm 0.8\ R_\odot$. However, using the surface

Table 5. Elemental abundances for BP Cir

Species	1 080 192			1 080 225			1 080 272		
	[El/H]	σ	NL	[El/H]	σ	NL	[El/H]	σ	NL
C I	−0.26	0.19	10	−0.17	0.12	10	−0.28	0.24	10
O I	+0.00	0.17	5	+0.06	0.13	2	+0.23	0.26	2
Na I	+0.17	0.22	7	−0.06	0.19	8	+0.09	0.26	7
Mg I	+0.06	0.29	5	−0.14	0.26	5	−0.12	0.35	4
Al I	+0.34	0.00	2	+0.49	0.18	2	+0.21	0.01	2
Si I	+0.07	0.14	18	+0.07	0.14	17	+0.05	0.13	21
Si II	+0.32	–	1	+0.06	0.29	2	−0.13	0.28	3
S I	+0.08	0.10	3	−0.01	0.26	4	−0.30	0.21	4
Ca I	−0.12	0.24	15	−0.02	0.21	17	−0.05	0.13	16
Sc I	+0.13	0.28	2	+0.18	0.31	3	+0.10	0.22	3
Sc II	−0.00	0.22	7	+0.19	0.19	9	+0.07	0.12	9
Ti I	+0.04	0.20	42	+0.07	0.20	56	+0.04	0.15	51
Ti II	+0.03	0.25	15	+0.09	0.11	17	+0.01	0.15	20
V I	+0.18	0.15	13	+0.15	0.14	9	+0.00	0.24	19
V II	+0.08	0.20	3	+0.03	0.05	5	+0.08	0.11	5
Cr I	+0.14	0.30	36	−0.01	0.19	45	+0.01	0.27	51
Cr II	+0.10	0.22	16	+0.06	0.19	18	+0.07	0.17	17
Mn I	−0.07	0.22	13	−0.08	0.24	15	−0.18	0.18	14
Fe I	+0.13	0.21	192	+0.13	0.18	187	+0.13	0.21	199
Fe II	+0.13	0.13	43	+0.13	0.13	42	+0.13	0.10	37
Co I	+0.19	0.18	17	+0.31	0.12	19	−0.04	0.22	23
Ni I	−0.05	0.22	77	−0.02	0.21	91	−0.03	0.21	95
Cu I	+0.05	0.13	4	+0.28	0.13	4	+0.27	0.17	3
Zn I	−0.38	0.42	3	−0.19	0.39	3	−0.49	0.19	4
Sr I	−0.19	–	1	+0.18	0.19	2	+0.17	0.32	4
Y I	–	–	–	–	–	–	+0.14	–	1
Y II	+0.14	0.14	9	+0.23	0.15	11	+0.14	0.19	11
Zr II	+0.11	0.24	4	+0.32	0.19	5	+0.10	0.27	6
Ru I	+0.38	–	1	–	–	–	–	–	–
La II	+0.16	0.33	6	+0.20	0.39	5	+0.22	0.17	8
Ce II	+0.15	0.25	10	+0.06	0.26	13	+0.08	0.17	12
Pr II	+0.00	0.10	3	+0.10	0.23	4	−0.15	0.14	2
Nd II	+0.25	0.25	17	−0.01	0.24	11	+0.21	0.14	15
Sm II	+0.07	0.13	3	+0.15	0.17	3	+0.15	0.20	3
Eu II	+0.28	0.07	2	+0.32	0.32	2	+0.33	0.12	2
Gd II	+0.29	–	1	+0.47	–	1	+0.12	–	1

Table 6. Averaged elemental abundances for BP Cir

Species	Our paper			LL	LAKGG
	[El/H]	σ	NL	[El/H]	[El/H]
C I	−0.24	0.18	30	−0.17	−0.24
O I	+0.06	0.18	9	+0.16	−0.18
Na I	+0.06	0.22	22	+0.12	+0.14
Mg I	−0.06	0.30	14	+0.11	−0.07
Al I	+0.35	0.06	6	−0.05	+0.01
Si I	+0.06	0.14	56	+0.10	+0.05
Si II	+0.01	0.24	6	–	–
S I	−0.09	0.20	11	–	+0.11
Ca I	−0.06	0.19	48	−0.06	−0.14
Sc I	+0.14	0.27	8	–	−0.11
Sc II	+0.09	0.17	25	–	–
Ti I	+0.05	0.14	149	+0.13	−0.13
Ti II	+0.04	0.17	52	–	–
V I	+0.09	0.19	41	–	−0.11
V II	+0.06	0.11	13	–	–
Cr I	+0.04	0.25	132	−0.07	−0.11
Cr II	+0.08	0.19	51	–	–
Mn I	−0.11	0.25	42	−0.19	−0.20
Fe I	+0.13	0.20	578	+0.02	−0.06
Fe II	+0.13	0.12	122	–	–
Co I	+0.14	0.18	59	+0.02	−0.22
Ni I	−0.03	0.21	263	−0.13	−0.08
Cu I	+0.19	0.14	11	–	+0.08
Zn I	−0.27	0.32	10	–	−0.19
Sr I	+0.12	0.24	7	–	–
Y I	+0.14	–	1	+0.14	+0.09
Y II	+0.17	0.16	31	–	–
Zr II	+0.18	0.17	15	–	+0.04
Ru I	+0.38	–	1	–	–
La II	+0.20	0.28	19	+0.22	+0.05
Ce II	+0.09	0.23	35	+0.03	+0.11
Pr II	+0.01	0.17	9	−0.17	−0.25
Nd II	+0.17	0.21	43	+0.03	−0.03
Sm II	+0.12	0.17	9	−0.06	−0.12
Eu II	+0.31	0.17	6	−0.15	+0.12
Gd II	+0.29	–	3	–	–

LL—data from Luck and Lambert (2011); LAKGG—data from Luck et al. (2011).

brightness method, Gieren (1984) determined its radius, $24.7 \pm 1.9\ R_\odot$, and distance, 528 ± 40 pc. According to the model by Cox (1979), R TrA with the mean $T_{\rm eff} = 6029$ K, a theoretical mass of 5.42 $M_\odot$, and the mass of 5.66 $M_\odot$ derived from the radius determined by the Baade–Wesselink method pulsates in the *fundamental mode*. According to the studies of Gieren (1981, 1982) and Lloyd Evans (1982) based on photometric data and radial velocity variations, the Cepheid is a binary system. Having analyzed the $O-C$ residuals, Szabados (1989) determined its orbital period, 3500 days. IRAS observations (McAllary and Welch 1986) revealed an infrared excess in R TrA due to the presence of silicate dust heated to 150–200 K around the Cepheid. The mean $T_{\rm eff}$ was estimated to be 6140 K, the mass of the dust and gas in this envelope are 7.8×10^{-9} and 8×10^{-7} $M_\odot$, respectively, and the mass loss rate by the Cepheid is $4 \times 10^{-9}\ M_\odot\ {\rm yr}^{-1}$. IUE observations (Evans 1995) allowed an upper limit for the spectral type of the companion to be determined, A4–A5 V. According to Böhm-Vitense (1988), R TrA pulsates in the *fundamental mode*.

Nardetto et al. (2006) took 14 spectra for R TrA with the 3.6-m telescope (HARPS spectrometer) at the La Silla Observatory (resolution $R = 120\,000$) to investigate the physical processes in the Cepheid's atmosphere. They found the mean $T_{\rm eff} = 6354$ K and $\log g = 2.0$ as well as the rather high projected rotation velocity $V_{\rm rot} \sin i = 16$ km s^{-1} using Kurucz's model atmospheres. The authors explained the change in the asymmetry of absorption lines with phase as the "cross of the compression wave just after the maximum contraction velocity."

The atmospheric parameters derived from only one spectrum at phase $0\overset{P}{.}167$ in LL and LAKGG are: $T_{\rm eff} = 6111 \pm 58$ and 6121 ± 72 K, $\log g = 2.47$ and 2.20, and $V_t = 4.01$ and 3.80 km s^{-1}, respectively. Our spectrum was taken at phase $0\overset{P}{.}766$ for a lower effective temperature and surface gravity (see Table 2).

The results of our abundance determinations for R TrA are presented in Table 7. It can be clearly seen that the iron abundance [Fe/H] = +0.09 dex is close to that in LAKGG (+0.06 dex). Our estimate shows a larger carbon underabundance than that in LL and LAKGG, our oxygen abundance is nearly solar and slightly differs from the LAKGG value. The estimates roughly coincide for sodium and larger than those in LL and LAKGG for magnesium and aluminum.

The abundances for the α-elements and Fe-peak elements are approximately identical, except for sulfur: there is a noticeable overabundance in LAKGG. For the r-process elements and heavy and light s-process elements, there are differences only

Table 7. Elemental abundances for R TrA

Species	R TrA (1010067)			LL	LAKGG
	[El/H]	σ	NL	[El/H]	[El/H]
C I	−0.46	0.16	15	−0.26	−0.23
O I	+0.06	0.18	4	+0.23	−0.08
Na I	+0.32	0.21	5	+0.49	+0.26
Mg I	+0.31	0.37	5	+0.21	+0.08
Al I	+0.40	0.21	3	+0.12	+0.14
Si I	+0.11	0.11	26	+0.23	+0.18
Si II	+0.35	–	1	–	–
S I	+0.06	0.14	5	–	+0.29
K I	+0.41	–	1	–	–
Ca I	+0.02	0.22	13	+0.10	+0.04
Sc I	+0.07	0.28	4	–	+0.04
Sc II	−0.08	0.21	7	–	–
Ti I	+0.04	0.21	64	+0.22	+0.10
Ti II	+0.04	0.16	11	–	–
V I	+0.11	0.17	19	–	+0.16
V II	+0.01	0.26	5	–	–
Cr I	+0.05	0.21	60	+0.11	+0.07
Cr II	+0.09	0.13	11	–	–
Mn I	−0.01	0.16	17	+0.02	+0.03
Fe I	+0.09	0.16	229	+0.19	+0.06
Fe II	+0.09	0.19	45	–	–
Co I	−0.04	0.16	29	+0.05	−0.07
Ni I	−0.01	0.19	104	−0.01	+0.00
Cu I	+0.28	0.40	4	–	+0.18
Zn I	+0.02	0.40	4	–	+0.03
Sr I	+0.43	0.34	3	–	–
Y II	+0.14	0.28	7	+0.29	+0.18
Zr II	+0.12	0.19	6	–	−0.16
Ru I	+0.53	–	1	–	–
La II	+0.24	0.27	6	+0.51	+0.27
Ce II	−0.02	0.18	10	+0.29	+0.11
Pr II	−0.07	0.54	2	−0.10	−0.33
Nd II	+0.13	0.28	16	+0.32	+0.69
Sm II	−0.03	0.12	3	+0.31	+0.15
Eu II	+0.20	0.12	2	+0.47	+0.14
Gd II	−0.45	–	1	–	–

LL—data from Luck and Lambert (2011); LAKGG—data from Luck et al. (2011).

in praseodymium and neodymium abundances (our values are closer to the solar ones). By analogy with the preceding objects, if we also take our results on the carbon and oxygen abundances as the main ones and add the LL and LAKGG estimates for nitrogen ([N/H] $\approx +0.36$ dex) to them, then it also turns out that R TrA has already passed the first dredge-up.

S TrA. This is a classical Cepheid of spectral type F8 II. Its main studies were performed by means of photometry (see Stobie 1970; Janot-Pacheco 1976; Eggen 1985b). Just as for R TrA, the maximum likelihood method (Balona 1977; Balona and Stobie 1979b) applied to analyze the Cepheid's radial velocities revealed that it is a radial pulsator with a mean radius $54.6 \pm 0.7\ R_\odot$. Similarly, the pulsation model by Cox (1979) for S TrA with the mean $T_{\rm eff} = 5682$ K, a theoretical mass of $6.46\ M_\odot$, and the mass of $6.40\ M_\odot$ determined from the radius estimated by the Baade–Wesselink method also pulsates in the *fundamental mode*. It was suspected of binarity from the radial velocity variations (Lloyd Evans 1982; Gieren 1982). According to Szabados (1989), who analyzed the $O-C$ residuals, the probable companion is present, but its orbital period is difficult to establish. IRAS observations (McAllary and Welch 1986) revealed no significant infrared excess in S TrA. IUE observations (Evans 1992) allowed an upper limit for the companion's spectral type to be determined, A3 V. According to Böhm-Vitense (1988), S TrA pulsates in the *fundamental mode*. Gieren (1984) found a radius of $38.6 \pm 2.9\ R_\odot$ and a distance of 731 ± 54 pc for the Cepheid by the surface brightness method.

Nielson and Lester (2008) computed a mass loss model for the Cepheid in the case of a radial pulsation. At the specified mean $T_{\rm eff} = 6230$ K, a mass of $2.8\ M_\odot$, and a radius of $39.2\ R_\odot$, the mass loss rate is 2.1×10^{-10} yr^{-1}.

We took one of the spectra for S TrA previously (Usenko et al. 2011) at phase $0\overset{P}{.}240$ ($T_{\rm eff} = 5857 \pm 28$ K, $\log g = 2.80$, $V_t = 4.70$ km s^{-1}). The abundance estimates are given in the above paper in Table 3. Based on only one spectrum at phase $0\overset{P}{.}176$, LL and LAKGG obtained the following atmospheric parameters: $T_{\rm eff} = 5962 \pm 58$ and 5976 ± 67 K, $\log g = 2.73$ and 2.10, and $V_t = 5.40$ and 4.20 km s^{-1}, respectively. In this paper, our spectrum was taken at phase $0\overset{P}{.}788$ and the effective temperature and the surface gravity have lower values (see Table 2).

The results of our abundance determinations for S TrA are presented in Table 8 (the data from spectrum 1 010 067 and those averaged over our two spectra). First of all, it should be noted that the iron abundance [Fe/H] $= +0.13$ dex is almost equal to that in LAKGG (+0.12 dex). Just as for R TrA, our estimate shows a larger carbon underabundance than

Table 8. Elemental abundances for S TrA

Species	S TrA (1010067)			S TrA (Mean)			LL	LAKGG
	[El/H]	σ	NL	[El/H]	σ	NL	[El/H]	[El/H]
C I	−0.22	0.11	13	−0.20	0.15	26	−0.15	−0.08
O I	+0.01	0.10	4	+0.01	0.12	7	+0.22	−0.13
Na I	+0.19	0.26	6	+0.22	0.27	11	+0.41	+0.28
Mg I	+0.05	0.21	3	−0.13	0.17	6	+0.28	−0.01
Al I	+0.28	0.23	3	+0.22	0.25	6	+0.16	+0.15
Si I	+0.08	0.15	25	+0.11	0.15	49	+0.14	+0.12
Si II	+0.01	0.24	2	+0.11	0.08	3	–	–
S I	−0.09	0.13	7	+0.07	0.18	13	–	+0.28
K I	−0.44	–	1	+0.46	–	2	–	–
Ca I	−0.19	0.19	11	−0.12	0.16	22	−0.03	+0.04
Sc I	+0.08	0.15	5	+0.06	0.13	10	–	+0.12
Sc II	−0.05	0.14	5	+0.01	0.14	11	–	–
Ti I	+0.03	0.21	63	+0.05	0.23	131	+0.14	+0.12
Ti II	−0.05	0.20	10	−0.02	0.23	23	–	–
V I	−0.05	0.24	25	−0.02	0.23	43	–	+0.09
V II	+0.01	0.21	5	+0.03	0.18	12	–	–
Cr I	+0.04	0.25	61	+0.05	0.24	111	+0.03	+0.07
Cr II	+0.13	0.18	9	+0.08	0.24	25	–	–
Mn I	−0.04	0.25	18	−0.10	0.22	33	−0.13	+0.04
Fe I	+0.12	0.20	217	+0.12	0.17	449	+0.21	+0.12
Fe II	+0.12	0.15	43	+0.12	0.16	83	–	–
Co I	−0.02	0.26	37	+0.05	0.23	70	+0.06	−0.07
Ni I	−0.06	0.18	79	−0.03	0.18	175	−0.03	+0.06
Cu I	−0.16	0.13	3	+0.04	0.12	7	–	+0.07
Zn I	−0.07	0.32	3	+0.07	0.41	5	–	–
Sr I	+0.05	0.11	2	+0.11	0.19	5	–	–
Y II	+0.08	0.15	5	+0.17	0.16	11	+0.28	+0.30
Zr II	+0.06	0.24	6	+0.18	0.23	11	–	+0.20
Ru I	–	–	–	+0.51	0.40	2	–	–
La II	+0.29	0.26	5	+0.19	0.24	10	+0.35	+0.31
Ce II	−0.04	0.26	13	+0.03	0.25	25	+0.17	+0.16
Pr II	+0.26	0.49	2	+0.23	0.17	4	+0.03	−0.17
Nd II	+0.04	0.27	14	+0.02	0.23	32	+0.21	+0.07
Sm II	−0.14	0.31	4	−0.09	0.26	6	+0.20	–
Eu II	+0.18	0.12	3	+0.22	0.10	6	+0.30	+0.17
Gd II	+0.34	–	1	+0.16	–	2	–	–

LL—data from Luck and Lambert (2011); LAKGG—data from Luck et al. (2011).

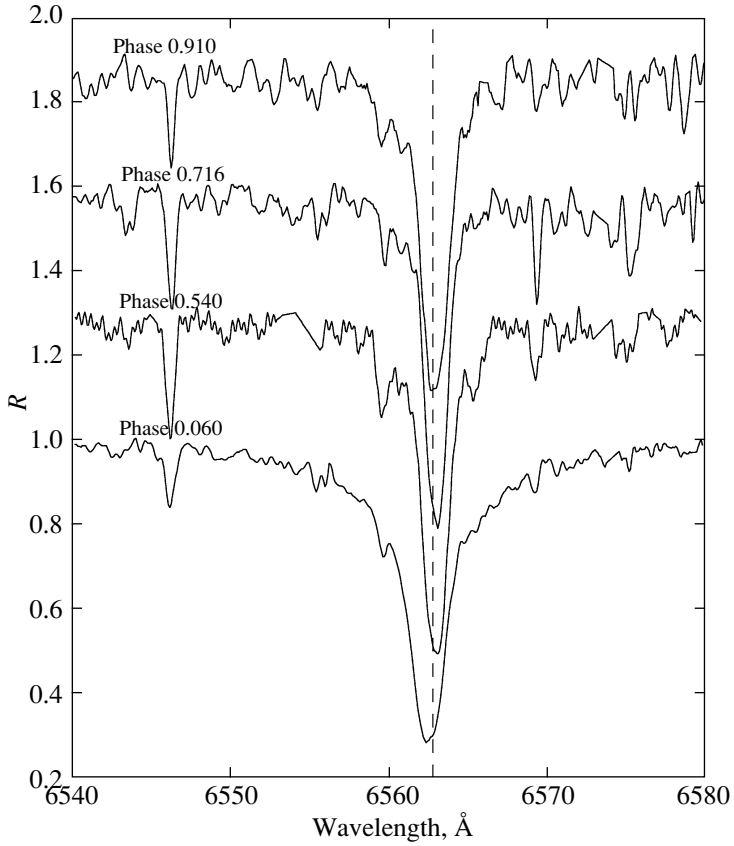

Fig. 5. Change of the Hα line profile with pulsation phase for U TrA.

that in LL and LAKGG, our oxygen abundance is also nearly solar, while there is a large underabundance in LAKGG. The estimates for the sodium abundance are approximately identical, for magnesium we obtained its underabundance, and for aluminum our value is slightly larger than that in LL and LAKGG.

The abundances for the α-elements and Fe-peak elements are approximately identical, except for sulfur: there is a noticeable overabundance in LAKGG. Our calcium and sulfur abundance estimates are slightly lower. For the r-process elements and heavy and light s-process elements, there are differences only in lanthanum and praseodymium abundances (our values are lower and closer to the solar estimates). Just as in the previous case, if we take our results on the carbon and oxygen abundances as the main ones and add the LL and LAKGG estimates for nitrogen ([N/H] $\approx +0.40$ dex) to them, then it can be concluded that S TrA has already passed the first dredge-up.

U TrA. This is one of the double-mode Cepheids (CEP(B)) of spectral type F8 Ib/II. In the presence of a $2\overset{\mathrm{d}}{.}57$ period in the *fundamental mode*, it exhibits variability with a *beat* period of $6\overset{\mathrm{d}}{.}304$. According to Jansen (1962), the ratio $P_1/P_0 = 0.7105$, hence the *first-overtone* period is $P_1 = 1\overset{\mathrm{d}}{.}825$.

It was investigated mainly photometrically (see Faulkner and Shobbrook 1979). Its mass, radius, and effective temperature were calculated from theoretical models: according to Petersen (1973), $M = 1.4\ M_\odot$ and $R = 17.3\ R_\odot$; according to King et al. (1975) (the model for $X = 0.7$ and $Z = 0.02$), $T_{\rm eff} = 5800 \pm 100$ K and $R = 18.8\ R_\odot$ and the Cepheid was near the red edge of the instability strip.

Its spectroscopic studies were first carried out by Rodgers and Gingold (1973). The authors found $T_{\rm eff} = 6146$ K and $\log g = 2.1 \pm 0.6$ using the curve-of-growth method. Based on these data, Cogan (1977) computed a model for U TrA with a convective zone. The Cepheid's mass in the model turned out to be 4 $M_\odot$. Subsequently, Cox et al. (1977a, 1977b) computed models for the Cepheid with $M = 1.2 \pm 0.2\ M_\odot$, $R = 17 \pm 1\ R_\odot$ (the case with $T_{\rm eff} = 6100$ K) and $M_{\rm th} = 4.6{-}4.9\ M_\odot$, $M_{\rm beat} = 1.2\ M_\odot$ (the case with $T_{\rm eff} = 6000$ K). According to Stobie (1977), the Cepheid has a mass of 1.3 $M_\odot$ and a radius $R = 16.9\ R_\odot$. Further studies of the radial velocities by means of Fourier analysis (Balona and Stobie 1979a,

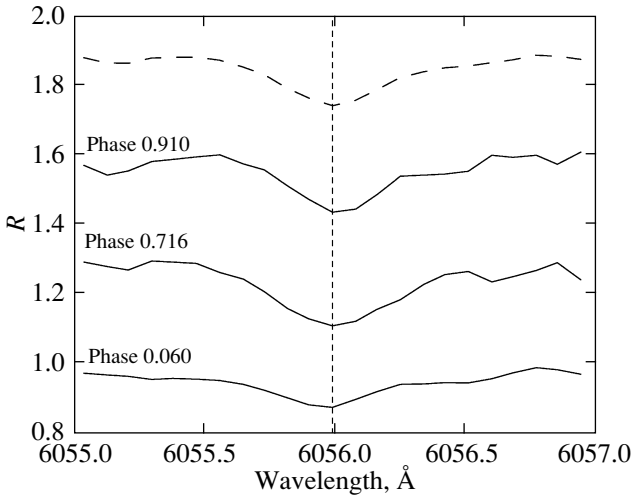

Fig. 6. Change of the Fe I 6055.99 Å absorption line profile with pulsation phase for U TrA. The averaged line profile obtained from our observational data is indicated by the dashed line in the upper part of the figure.

1979c) allowed the radii to be estimated by the Baade–Wesselink method, from 19.4 $R_\odot$ to 34.4 $R_\odot$.

Based on three spectra of the Cepheid near the Hα line, Barrell (1978) pointed out that the line profiles are sharp and symmetric at phases $0\overset{P}{.}14$ and $0\overset{P}{.}26$ and with a flat irregular core at phase $0\overset{P}{.}78$. Thereafter, she (Barrell 1981) determined the range of effective temperatures 5688–6237 K with the mean $T_{\rm eff} = 5957$ K using 17 spectra near the Hα line. Subsequently, however, Barrell (1982) found the following atmospheric parameters by the curve-of-growth method: $T_{\rm eff} = 6215$ K, $\log g = 2.35 \pm 0.5$, and $V_t = 4.80 \pm 0.1$ km s^{-1}, while [Fe/H] $= -0.02$ dex. Subsequently, no detailed spectroscopic studies of this double-mode Cepheid were carried out.

Having analyzed the photometric observations of U TrA by means of Fourier analysis, Faulkner and Shobbrook (1979) showed that the *fundamental pulsation period* decreases, while the *first-overtone* one increases. This led the authors to conclude that the star evolves toward the blue edge of the Cepheid instability strip. IUE observations (Evans 1992) revealed a companion to the Cepheid with an upper limit for the spectral type of A0 V.

We took four spectra at different phases of the light curve (see Tables 1 and 2). The atmospheric parameters and chemical composition were determined only from three spectra (see Table 2); spectrum 1 080 030 was excluded from our analysis, because it was very noisy. Our mean atmospheric parameters are $T_{\rm eff} = 6085 \pm 29$ K, $\log g = 2.00$, and $V_t = 3.90$ km s^{-1}. The effective temperature estimates are slightly lower than those in Rodgers and Gingold (1973) and Barrell (1982), while the surface gravity and microturbulent velocity estimates are close to the data of these authors. It should be noted that our values were found by the method of model atmospheres, in contrast to the curve-of-growth method applied by the previous authors.

Figure 5 also presents the Hα line profiles for the Cepheid at various pulsation phases. It can be seen that these profiles are not so symmetric at early phases as was described by Barrell (1978), while at phase $0\overset{P}{.}716$ (close to $0\overset{P}{.}78$) no flat irregular core is noticeable; something similar is observed at phase $0\overset{P}{.}910$. A difference in the radial velocities of the Hα line core is seen in the figure, which was not observed for the small-amplitude Cepheids AV Cir and BP Cir. Just as for the small-amplitude Cepheids, Figs. 6 and 7 present the Fe I 6055.99 Å, Fe II 6369.46 Å, and Si II 6371.355 Å line profiles, respectively, for three spectra of U TrA (spectrum 1 080 030 was not used, because it was very noisy). At some phases, the lines are asymmetric and this can be explained by the presence of nonradial pulsations in the double-mode Cepheid.

We have determined the abundances of chemical elements in the atmosphere of U TrA (except for iron) for the first time. As can be seen from Table 9, our mean estimate of [Fe/H] $= +0.01$ dex is close to that in Barrell (1982): -0.02 dex. Carbon is underabundant, the oxygen abundance is nearly solar, sodium is slightly overabundant and aluminium has a more noticeable overabundance, while the magnesium abundance is nearly solar. The abundances

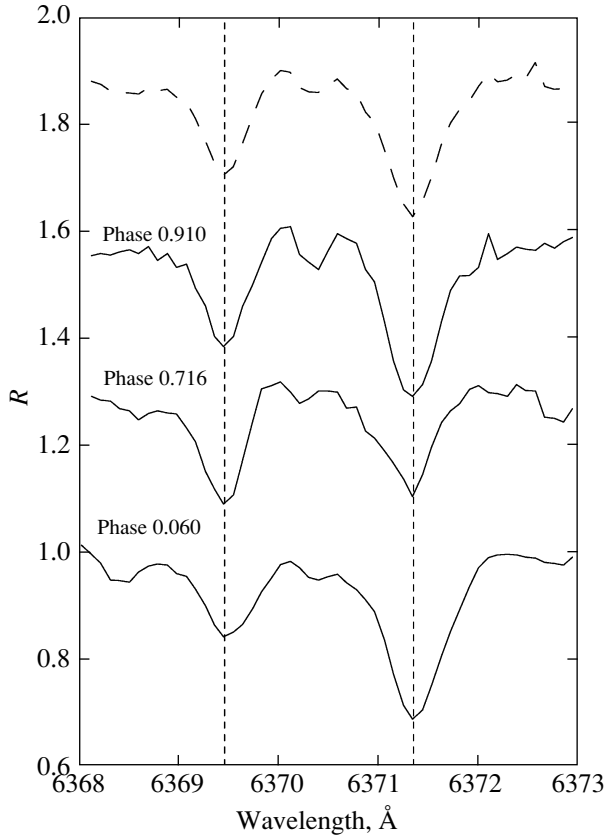

Fig. 7. Change of the Fe II 6369.46 Å and Si II 6371.355 Å absorption line profiles with pulsation phase for U TrA. The averaged line profile obtained from our observational data is indicated by the dashed line in the upper part of the figure.

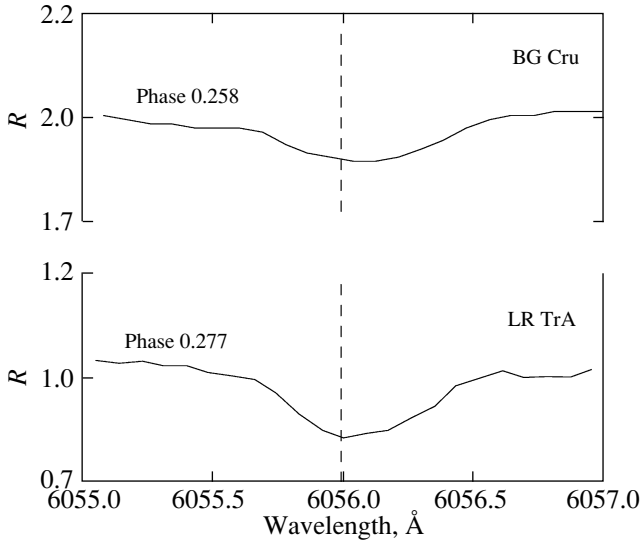

Fig. 8. Fe I 6055.99 Å absorption line profile for LR TrA. A similar profile for the small-amplitude Cepheid BG Cru at a close pulsation phase is presented for comparison.

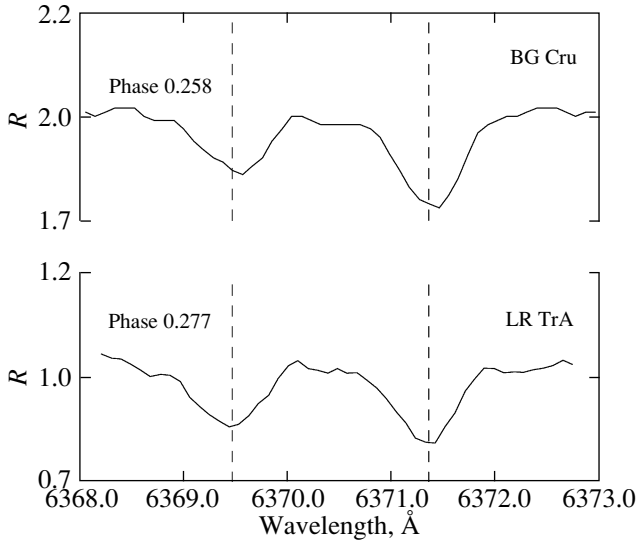

Fig. 9. Fe II 6369.46 Å and Si II 6371.355 Å absorption line profiles for LR TrA. A similar profile for the small-amplitude Cepheid BG Cru at a close pulsation phase is presented for comparison.

of the α-elements and Fe-peak elements show no significant deviations and are nearly solar. The same can also be said about the r-process elements and heavy and light s-process elements: their abundances are nearly solar, except for europium and gadolinium. Judging by the carbon, oxygen, and sodium abundance estimates, it can be surmised that U TrA also has passed the first dredge-up.

LR TrA. This small-amplitude Cepheid (DCEPS) of spectral type F8 II was discovered relatively recently (Eggen 1983) and was investigated mainly photometrically (Eggen 1985a, 1985b; Berdnikov and Pastukhova 1995). It was assigned to the DCEPS class by Antonello et al. (1990). According to Szabados et al. (2013) (IUE observations), a hot companion was detected in LR TrA.

Only one spectrum was taken by LL and LAKGG at phase $0\overset{P}{.}086$ with the atmospheric parameters $T_{\rm eff} = 5929 \pm 52$ and 5943 ± 117 K, $\log g = 2.31$ and 2.20, and $V_t = 5.13$ and 4.40 km s^{-1}, respectively. Our spectrum was taken at phase $0\overset{P}{.}277$, which roughly corresponds to the mean effective temperature (given the sinusoidal light curve of the small-amplitude Cepheid). The atmospheric parameters we determined are given in Table 2.

The absorption lines in the spectrum of LR TrA are highly unusual and have strong asymmetric profiles with the possible presence of additional components, as, for example, in BG Cru. Figures 8 and 9 show the already known Fe I 6055.99 Å, Fe II 6369.46 Å, and Si II 6371.355 Å absorption line profiles for LR TrA и BG Cru from the spectrograms taken at approximately close pulsation phases. The similarity is obvious. According to Usenko et al. (2014), the small-amplitude Cepheid BG Cru pulsates in the *first overtone* and has an extended gas envelope. It is quite obvious that LR TrA possesses the same characteristics.

If we compare our abundance data with those in LL and LAKGG, then it can be noticed that this small-amplitude Cepheid exhibits the largest metallicity: [Fe/H] = +0.20 dex in our paper (see Table 10), +0.31 dex in LL, and +0.25 dex in LAKGG. The carbon abundance (underabundance) coincides with the LL one, while LAKGG give its nearly solar abundance. The reverse is true for oxygen: our nearly solar abundance coincides with the LAKGG one, while it is enhanced in LL. Our sodium and magnesium abundances are noticeably lower than those in LL and LAKGG, while the aluminum abundance is much higher (Table 10).

The abundances of the α-elements and Fe-peak elements are approximately identical, except for sulfur, calcium, titanium, and nickel: they are noticeably overabundant in LL and LAKGG. Our estimates for the r-process elements and heavy and light s-process elements are different only in the abundances of copper (larger), lanthanum (smaller), praseodymium (larger), and europium (smaller). If we take our results on the carbon and oxygen abundances as the main ones and add the LL and LAKGG estimates for nitrogen to them (although they differ greatly: [N/H] from +0.41 dex in LL and +0.19 dex in LAKGG), then it can be surmised that LR TrA probably has also passed the first dredge-up.

Table 9. Elemental abundances for U TrA

Species	1 080 101			1 080 155			1 080 177			Mean		
	[El/H]	σ	NL	[El/H]	σ	NL	[El/H]	σ	NL	[El/H]	σ	NL
C I	−0.30	0.23	11	−0.36	0.23	12	−0.39	0.35	11	−0.35	0.23	34
O I	+0.00	0.05	2	−0.18	–	1	+0.21	0.06	3	+0.08	0.17	6
Na I	+0.29	0.28	6	+0.11	0.11	3	+0.02	0.21	6	+0.15	0.25	15
Mg I	+0.09	0.04	4	−0.04	0.33	5	−0.21	0.04	4	−0.05	0.23	13
Al I	−0.16	0.04	2	+0.23	0.02	2	+0.38	0.13	2	+0.30	0.32	6
Si I	+0.07	0.17	16	+0.07	0.22	16	−0.00	0.13	17	+0.05	0.16	49
Si II	–	–	–	−0.17	0.14	2	–	–	–	−0.17	0.14	2
S I	−0.04	0.29	4	−0.06	0.05	3	−0.04	0.24	5	−0.08	0.17	12
Ca I	+0.11	0.24	10	−0.00	0.15	10	−0.05	0.13	16	−0.02	0.15	36
Sc I	+0.19	0.02	2	(+0.47)	0.07	3	+0.29	0.09	2	+0.24	0.08	4
Sc II	−0.06	0.19	6	−0.17	0.21	9	−0.14	0.16	8	−0.12	0.17	23
Ti I	+0.07	0.20	29	+0.02	0.16	34	+0.01	0.21	36	+0.04	0.18	99
Ti II	−0.08	0.25	9	−0.11	0.11	8	−0.11	0.16	16	−0.10	0.15	33
V I	+0.13	0.24	9	+0.08	0.22	13	+0.03	0.21	7	+0.07	0.20	29
V II	−0.09	0.16	4	−0.02	0.08	4	−0.13	0.11	5	−0.08	0.12	13
Cr I	+0.09	0.20	37	−0.03	0.26	16	−0.09	0.23	42	−0.00	0.23	95
Cr II	−0.05	0.20	16	+0.01	0.23	13	−0.00	0.22	17	−0.01	0.21	46
Mn I	−0.07	0.26	13	−0.10	0.32	13	+0.06	0.25	12	−0.06	0.27	38
Fe I	+0.02	0.15	139	+0.01	0.19	153	+0.00	0.16	162	+0.01	0.17	454
Fe II	+0.02	0.14	29	+0.01	0.16	33	−0.00	0.12	33	+0.01	0.14	95
Co I	+0.11	0.25	14	−0.01	0.27	12	+0.10	0.17	14	+0.08	0.22	40
Ni I	+0.06	0.19	71	−0.04	0.21	52	−0.05	0.20	75	−0.02	0.20	198
Cu I	+0.17	0.26	3	−0.31	0.12	2	+0.27	0.28	4	+0.11	0.33	9
Zn I	−0.08	0.35	3	−0.05	–	1	−0.08	0.66	2	−0.08	0.37	6
Sr I	–	–	–	+0.17	0.76	2	+0.23	0.93	2	+0.20	0.69	4
Y II	+0.07	0.18	7	−0.12	0.24	8	−0.13	0.08	8	−0.08	0.18	23
Zr II	+0.01	0.23	5	−0.01	0.08	3	+0.15	0.26	7	+0.07	0.23	15
Ru I	–	–	–	+0.25	–	1	–	–	–	+0.25	–	1
Ba II	–	–	–	–	–	–	+0.08	–	1	+0.08	–	1
La II	+0.23	0.20	6	+0.17	0.18	3	+0.05	0.25	7	+0.14	0.22	16
Ce II	+0.03	0.21	8	−0.07	0.15	8	+0.04	0.23	10	−0.03	0.16	26
Pr II	−0.26	0.19	2	+0.01	–	1	−0.17	0.08	2	−0.17	0.15	5
Nd II	+0.16	0.14	19	+0.01	0.20	16	+0.05	0.24	13	+0.09	0.19	48
Sm II	−0.06	0.06	4	+0.08	0.47	2	+0.15	0.11	3	+0.04	0.21	9
Eu II	+0.17	–	1	–	–	–	+0.24	0.10	2	+0.22	0.08	3
Gd II	+0.41	–	1	–	–	–	+0.28	–	1	+0.35	0.09	2

Table 10. Elemental abundances for LR TrA

Species	LR TrA (1080237)			LL	LAKGG
	[El/H]	σ	NL	[El/H]	[El/H]
C I	−0.15	0.21	10	−0.15	+0.07
O I	−0.00	0.31	4	+0.21	+0.03
Na I	+0.08	0.25	5	+0.15	+0.28
Mg I	+0.19	0.29	4	+0.47	+0.27
Al I	+0.65	0.28	2	+0.36	+0.22
Si I	+0.13	0.17	18	+0.28	+0.19
Si II	+0.21	–	1	–	–
S I	−0.15	0.18	4	–	+0.34
Ca I	+0.08	0.25	9	+0.22	+0.17
Sc I	+0.31	0.30	4	–	+0.11
Sc II	+0.08	0.28	7	–	–
Ti I	+0.14	0.19	38	+0.28	+0.24
Ti II	+0.21	0.14	8	–	–
V I	+0.19	0.15	14	–	+0.18
V II	+0.03	0.21	3	–	–
Cr I	+0.09	0.25	43	+0.13	+0.21
Cr II	+0.11	0.26	13	–	–
Mn I	+0.11	0.23	13	+0.11	+0.11
Fe I	+0.20	0.18	156	+0.31	+0.25
Fe II	+0.20	0.18	30	–	–
Co I	+0.14	0.21	22	+0.21	+0.12
Ni I	+0.02	0.20	73	+0.14	+0.15
Cu I	+0.39	0.33	4	–	+0.13
Zn I	−0.13	0.43	4	–	+0.01
Sr I	+0.07	–	1	–	–
Y II	+0.30	0.30	6	+0.35	+0.26
Zr II	+0.19	0.26	4	–	+0.24
Ru I	+0.29	–	1	–	–
La II	+0.24	0.26	5	+0.56	+0.33
Ce II	+0.18	0.21	9	+0.16	+0.09
Pr II	+0.08	0.31	4	−0.04	−0.17
Nd II	+0.24	0.17	14	+0.27	+0.04
Sm II	+0.19	0.21	3	+0.25	–
Eu II	+0.11	0.10	2	+0.30	+0.22
Gd II	+0.37	–	1	–	+0.26

LL—data from Luck and Lambert (2011); LAKGG—data from Luck et al. (2011).

CONCLUSIONS

We took 13 spectra for three small-amplitude Cepheids (AV Cir, BP Cir, and LR TrA), two classical Cepheids (R TrA and S TrA), and one double-mode Cepheid (U TrA) with the the 1.9-m telescope of the South African Astronomical Observatory (South African Republic). The results of our reduction and analysis of the spectra obtained are as follows:

(1) We have been able to determine (for U TrA) or refine significantly (for the remaining objects) the atmospheric parameters and chemical composition of the program Cepheids for the first time.

(2) Our analysis of the chemical composition for these objects revealed a carbon underabundance, a nearly solar oxygen abundance, an overabundance of sodium and aluminum, and a nearly solar (or slightly enhanced) magnesium abundance, suggesting that these supergiants have already passed the first dredge-up. Our LTE estimates of the C, O, and Na abundances agree well with the results obtained by Takeda et al. (2013) for 12 Cepheids in the non-LTE approximation ([C/H] $\approx$ from −0.2 to −0.4 dex; [O/H] $\approx$ +0.0 dex; [Na/H] $\approx$ from +0.1 to +0.2 dex).

(3) The values of [Fe/H] for all of the program Cepheids are slightly higher than the solar ones, except for the double-mode Cepheid U TrA. The largest value of +0.20 dex was revealed for LR TrA. The metallicity estimates for the small-amplitude Cepheids AV Cir and BP Cir coincide. Since the Galactic coordinates of these objects are close, the assumption about their common genesis can be made. The same can also be said about the classical Cepheids R TrA and S TrA.

(4) The abundances of the α-elements, iron-peak elements, and r- and s-process elements turned out to be nearly solar (or slightly higher) for all Cepheids.

(5) Our abundance estimates are mostly consistent with the data obtained in LL and LAKGG for the α-elements, Fe-peak elements, r-process elements, and heavy and light s-process elements. Significant differences in [Fe/H] are observed for BP Cir. For the "key elements" of the evolution of yellow supergiants, there is a significant difference in carbon and oxygen abundances for AV Cir, R TrA, S TrA, and LR TrA; we obtained a noticeable C underabundance and a nearly solar O abundance, while the reverse is true in LL and LAKGG. It should be noted that our data for AV Cir, BP Cir, and S TrA were obtained from a larger number of spectra for each Cepheid and show closer values. In addition, we used a larger number of lines for carbon and oxygen in our analysis, suggesting that our data are more reliable.

(6) For the small-amplitude Cepheids AV Cir and BP Cir, the Hα line profiles are symmetric, except for

the slight asymmetry in the core at approximately the same phase near $0^P.7$: on the blue side for AV Cir and on the red one for BP Cir. The absorption lines of neutral atoms and ions at various pulsation phases are, on the whole, symmetric for AV Cir, while a distinct asymmetry is observed for BP Cir. It is quite probable that AV Cir exhibits radial pulsations, while BP Cir exhibits nonradial *first-overtone* pulsations, although the mean $\log g = 2.75$ more likely corresponds to the *fundamental mode*. The constancy of the Hα absorption line profiles with pulsation phase for both small-amplitude Cepheids may suggest the presence of a hydrogen envelope around them.

(7) The double-mode Cepheid U TrA exhibits an asymmetry in the cores of the Hα line and the absorption lines of neutral atoms and ions at various pulsation phases. This can be explained by the presence of nonradial pulsations in the Cepheid's atmosphere. The value of [Fe/H] = +0.01 dex that we determined by the method of model atmospheres turned out to be close to −0.02 dex determined previously by the curve-of-growth method.

(8) Judging by the absorption lines of metals (both neutral atoms and ions), the small-amplitude Cepheid LR TrA closely resembles the already known Cepheid BG Cru (Usenko et al. 2014): secondary "blue" and "red" components whose line depths vary with pulsation phase are noticeable in this small-amplitude Cepheid. We showed that BG Cru pulsates in the *first overtone* and that it has an extended hydrogen envelope. The same can probably be also said about LR TrA, but its careful multiphase spectroscopic observations with a sufficiently high resolution are highly needed for this purpose in future.

ACKNOWLEDGMENTS

This study was financially supported by the Russian Foundation for Basic Research (project no. 10-02-00489). The study was also supported by the South African National Research Foundation. I.A. Usenko is grateful to V.V. Kovtyukh for his help in preparing the reduction of spectroscopic data.

REFERENCES

1. E. Antonello, E. Poretti, and L. Reduzzi, Astron. Astrophys. **236**, 138 (1990).
2. A. Arellano Ferro, Mon. Not. R. Astron. Soc. **209**, 481 (1984).
3. A. Arellano Ferro and B. F. Madore, Observ. **105**, 207 (1985).
4. L. A. Balona, Mon. Not. R. Astron. Soc. **178**, 231 (1977).
5. L. A. Balona, Observ. **101**, 205 (1981).
6. L. A. Balona, Internal SAAO Rep. (SAAO, Capetown, 1999), p. 1.
7. L. A. Balona and R. S. Stobie, Mon. Not. R. Astron. Soc. **189**, 627 (1979a).
8. L. A. Balona and R. S. Stobie, Mon. Not. R. Astron. Soc. **189**, 649 (1979b).
9. L. A. Balona and R. S. Stobie, Mon. Not. R. Astron. Soc. **189**, 659 (1979c).
10. S. L. Barrell, Astrophys. J. **226**, L141 (1978).
11. S. L. Barrell, Mon. Not. R. Astron. Soc. **196**, 357 (1981).
12. S. L. Barrell, Mon. Not. R. Astron. Soc. **200**, 177 (1982).
13. J. Baudrand and T. Böhm, Astron. Astrophys. **259**, 711 (1992).
14. L. N. Berdnikov and E. N. Pastukhova, Astron. Lett. **21**, 368 (1995).
15. L. N. Berdnikov and D. G. Turner, Astrophys. J. Suppl. Ser. **137**, 209 (2001).
16. L. N. Berdnikov, A. Yu. Knyizev, I. A. Usenko, V. V. Kovtyukh, and V. V. Kravtsov, Astron. Lett. **36**, 490 (2010).
17. E. Böhm-Vitense, Astrophys. J. **324**, L27 (1988).
18. B. C. Cogan, Astrophys. J. **211**, 890 (1977).
19. A. N. Cox, Astrophys. J. **229**, 212 (1979).
20. A. N. Cox, D. S. King, S. W. Hodson, and A. A. Henden, Astrophys. J. **212**, 451 (1977a).
21. A. N. Cox, R. G. Deupree, D. S. King, and S. W. Hodson, Astrophys. J. **214**, L127 (1977b).
22. H. Dekker, S. D'Odorico, A. Kaufer, B. Delabre, and H. Kotzlowski, Proc. SPIE **4008**, 534 (2000).
23. O. J. Eggen, Astron. J. **88**, 361 (1983).
24. O. J. Eggen, Astron. J. **90**, 1260 (1985a).
25. O. J. Eggen, Astron. J. **90**, 1297 (1985b).
26. N. R. Evans, Astrophys. J. **384**, 220 (1992).
27. N. R. Evans, Astrophys. J. **436**, 273 (1994).
28. N. R. Evans, Astrophys. J. **445**, 393 (1995).
29. N. R. Evans, A. Arellano Ferro, and J. Udalska, Astron. J. **103**, 1638 (1992).
30. D. J. Faulkner and R. R. Shobbrook, Astrophys. J. **232**, 197 (1979).
31. G. A. Galazutdinov, Publ. SAO RAN **92**, 1 (1992).
32. W. Gieren, Rev. Mex. Astr. Astrophys. **6**, 103 (1981).
33. W. Gieren, Astrophys. J. **260**, 208 (1982).
34. W. Gieren, Astrophys. J. **282**, 650 (1984).
35. C. A. Iglesias and F. J. Rogers, Astrophys. J. **378**, 408 (1991).
36. E. Janot-Pacheco, Astron. Astrophys. **25**, 159 (1976).
37. A. G. Jansen, Bull. Inst. Astron. Neth. **16**, 141 (1962).
38. P. N. Kholopov, N. N. Samus', M. S. Frolov, et al., *General Catalog of Variable Stars* (Nauka, Moscow, 1986), vol. 3 [in Russian].
39. P. S. King, C. J. Hansen, R. R. Ross, and J. P. Cox, Astrophys. J. **195**, 467 (1975).
40. A. Y. Kniazev, S. A. Pustilnik, E. K. Grebel, H. Lee, and A. G. Pramskij, Astrophys. J. Suppl. Ser. **153**, 429 (2004).
41. V. V. Kovtyukh, Mon. Not. R. Astron. Soc. **378**, 617 (2007).
42. D. W. Kurtz, Mon. Not. Astron. Soc. South. Africa **38**, 36 (1979).

43. R. L. Kurucz, in *Proceedings of the IAU Symposium No. 149 on Model Atmospheres for Populational Synthesis. The Stellar Populations of Galaxies,* Ed. B. Barbuy and A. Renzini (Kluwer Academic, Dordrecht, 1992), p. 225.
44. T. Lloyd Evans, Mon. Not. R. Astron. Soc. **199**, 925 (1982).
45. R. E. Luck, S. M. Andrievsky, V. V. Kovtyukh, W. Gieren, and D. Graczyk, Astron. J. **142**, 51 (2011).
46. R. E. Luck and D. L. Lambert, Astron. J. **142**, 136 (2011).
47. C. W. McAllary and D. L. Welch, Astron. J. **91**, 1209 (1986).
48. N. Nardetto, D. Mourad, P. Kervella, Ph. Mathias, A. Merand, and D. Bersier, Astron. Astrophys. **453**, 309 (2006).
49. H. R. Nielson and J. B. Lester, Astrophys. J. **684**, 569 (2008).
50. E. H. Olsen, Astrophys. J. Suppl. Ser. **37**, 367 (1979).
51. J. O. Petersen, Astron. Astrophys. **27**, 89 (1973).
52. O. K. L. Petterson, P. L. Cotterell, and M. D. Albrow, Mon. Not. R. Astron. Soc. **350**, 95 (2004).
53. O. K. L. Petterson, P. L. Cotterell, M. D. Albrow, and A. B. Fokin, Mon. Not. R. Astron. Soc. **365**, 1167 (2005).
54. A. W. Rodgers and R. A. Gingold, Mon. Not. R. Astron. Soc. **161**, 23 (1973).
55. E. G. Schmidt, Astrophys. J. **162**, 871 (1970).
56. R. S. Stobie, Mon. Not. R. Astron. Soc. **148**, 1 (1970).
57. R. S. Stobie, Mon. Not. R. Astron. Soc. **180**, 631 (1977).
58. L. Szabados, Budapest. Mitt. **11** (pt. 1, No. 94), 1 (1989).
59. L. Szabados, R. I. Anderson, A. Derekas, L. L. Kiss, T. Szalai, P. Székely, and J. L. Christiansen, Mon. Not. R. Astron. Soc. **434**, 870 (2013).
60. Y. Takeda, D.-I. Kang, I. Han, B.-C. Lee, and K.-M. Kim, Mon. Not. R. Astron. Soc. **432**, 769 (2013).
61. I. A. Usenko, A. Yu. Kniazev, L. N. Berdnikov, and V. V. Kravtsov, Astron. Lett. **37**, 499 (2011).
62. I. A. Usenko, A. Yu. Kniazev, L. N. Berdnikov, V. V. Kravtsov, and A. B. Fokin, Astron. Lett. **39**, 432 (2013).
63. I. A. Usenko, V. G. Klochkova, and N. S. Tavolzhanskaya, Astron. Lett. **39**, 634 (2013a).
64. I. A. Usenko, A. Yu. Kniazev, L. N. Berdnikov, A. B. Fokin, and V. V. Kravtsov, Astron. Lett. **40**, 435 (2014).

Translated by V. Astakhov